The thermoelectric power factor enhancement of $GaAs_{1-x}N_x$

Y. YILDIZ[a], K. BILEN[a], M. BOSI[b], A. YILDIZ[c,*]
[a]*Department of Mechanical Engineering, Faculty of Engineering and Natural Sciences, Ankara Yıldırım Beyazıt University, Ankara, Turkey*
[b]*CNR-IMEM Institute, Area delle Scienze 37/A, I-43124, Parma, Italy*
[c]*Department of Energy Systems Engineering, Faculty of Engineering and Natural Sciences, Ankara Yıldırım Beyazıt University, Ankara, Turkey*

We investigated the application of undoped and Si-doped GaAsN samples grown by a metal organic vapor phase epitaxy (MOVPE) technique on semi-insulating (SI) and *n*-type GaAs substrates as a novel thermoelectric material. The structural and optical properties of the samples were characterized by XRD and photoluminescence (PL) measurements, respectively. Hall effect measurements were made as a function of temperature. The effects of the layer structure and growth conditions of the samples on the thermoelectric performance of GaAsN were demonstrated by obtaining values of the power factor (*PF*). The results show that Si doping has a substantial influence on the *PF* of GaAsN, indicating that Si-doped GaAsN might be a promising candidate for thermoelectric energy harvesters.

(Received January 22, 2018; accepted October 10, 2018)

Keywords: GaAsN; MOVPE; Power factor; Thermoelectric properties

1. Introduction

One of today's most important challenges is discovering how to obtain clean, eco-friendly and renewable energy since the majority of the world's population is using fossil fuels that release harmful greenhouse gases and are, in addition, being depleted. To benefit from *waste energy*, a type of energy released from generators, vibration, heat engines, and moving parts or fluids, devices based on thermoelectric materials (TMs) are considered. Thermoelectric materials such as Bi_2Te_3, PbTe, SiGe, and BiSb are used to convert thermal energy into electrical energy without any emission of greenhouse gases and have therefore attracted wide interest in recent years [1,2]. A high value of power factor ($PF = S^2ne\mu$, where *S* is Seebeck coefficient, *n* is carrier concentration, *e* is charge of electron, and μ is mobility) indicates a high conversion efficiency in TMs. To obtain a high *PF*, degenerate semiconductors are usually considered, in which the Fermi level is well above the conduction band edge for the *n-type* [3-5].

Many efforts have been made to boost the thermoelectric performance of various materials and to discover new candidates for thermoelectrics with high *PF* values [6-10]. High performance thermoelectric semiconductor materials can possess a *PF* value varying between 5 and 8000 W/mK^2 [6, 7]. For example, Han et *al.* [8] reported exceptional *PF* values that varied between 28-40 $\mu W/mK^2$ at 300 K for SnSe samples. Wang et al. [9] obtained *PF* values as high as 19 $\mu W/mK^2$ at 300 K for polyaniline/graphene nanocomposite films among the reported polymer/graphene TE composites [9]. The effects of crystal anisotropy on the thermoelectric properties of textured $KSr_2Nb_5O_{15}$ ferroelectric ceramics were studied by Duran et al. [1] and found to result in a *PF* value of 390 $\mu W/mK^2$ at 1120 K. Wan et *al.* [10] investigated TiS_2, which has applications in wearable electronics, and reported a *PF* value of 450 $\mu W/mK^2$ at 373 K.

Dilute $GaAs_{1-x}N_x$ alloys have attracted increasing interest for potential electronic and photonic device applications due to their optical and electrical properties. The addition of a small amount of nitrogen to GaAs leads to unexpectedly strong modifications of optical and electrical properties. Most work on $GaAs_{1-x}N_x$ alloys has focused on band gap bowing, effective mass, and the effects of nitrogen on optical properties. However, only a few studies have been conducted on their electrical and thermoelectric characteristics [11-16].

To better understand the electrical and thermoelectric characteristics of $GaAs_{1-x}N_x$ alloys, we have in this study performed temperature dependent Hall effect measurements and calculations of the power factor. To the best of our knowledge, this is the first observation of the thermoelectric properties of GaAsN in the literature. Our work, for the first time, explores the layer structure and growth conditions of GaAsN, which can be considered a novel thermoelectric material, through theoretical calculations and experimental verification.

2. Experimental

The samples were grown in a horizontal MOVPE reactor heated by IR lamps at pressures of 100 and 750 Torr. Trimethylgallium (TMG), arsine (AsH_3) and dimethylhidrazine (DMHy) diluted in 2000 sccm

palladium-purified H_2 carrier gas were used as Ga, As and N precursors, respectively. $GaAs_{1-x}N_x$ layers were deposited at 515-530 ^{0}C on a 50 nm-thick GaAs buffer layer grown at 600 ^{0}C. Detailed growth parameters are shown in Table 1. The sample with x=2.98% is grown on a 350 μm thick Si doped (1-3x10^{18} cm^{-3}) (100) GaAs substrate (*n*-type), misoriented 2° towards the [110] direction. The other samples, x= 3.01% and 2.91%, are grown on a 450 μm thick SI (100) GaAs substrate. The thickness of the GaAsN layers is in the range of 350 - 400 nm, depending on the growth parameters. The sample with x=2.91% was a doped *n*-type using a SiH_4 flow during the growth process. The layer structures of the samples are given in Fig. 1.

Table 1. Growth parameters of the samples

Parameters	**x= 2.98%**	**x= 3.01%**	**x= 2.91%**
Growth Temp. (^{o}C)	530	515	515
React. Press. (Torr)	750	100	100
DMHy/V	7.18	7.47	8.89
X_V	0.93	0.93	0.95
V/III	921	1591	1858
DMHy/III	800	1403	1671

(a) *(b)* *(c)*

Fig. 1. Layer structure of the samples; with (a) x= 2.98%, (b) x= 3.01%, and (c) x= 2.91%

The XRD measurements were performed by a D8-DISCOVER diffractometer equipped on the primary side with a Ge (220) monochromator. The Hall effect measurements were made in steps over a temperature range of 20-305 K using a Lake Shore Hall effect measurement system. Room temperature PL measurements were conducted using the Jobin Yvon Florog-550 system with a 55 mW He-Cd laser (325 nm) used as a light.

3. Results and discussion

Fig. 2 shows the XRD patterns of the samples. Analysis of the XRD data for the samples indicates the presence of two different crystalline phases. One peak, which is about 33^o, corresponds to GaAs, while the other one which is a little away, indicates $GaAs_{1-x}N_x$. The position of the $GaAs_{1-x}N_x$ peak depends on the average nitrogen concentration, demonstrating a slight change in the nitrogen composition (x) of the samples. To determine the nitrogen concentration of the samples, the XRD data is simulated with software based on XRD. The values of x are calculated through a simulation using a commercial LEPTOS [17] program used for the analytical interpretation of data obtained in glancing-incidence X-ray reflectivity and high-resolution X-ray diffraction experiments on thin film structures that is based on Vegard's law [18-19]. Accurate results were obtained by simulating the (002) diffraction peaks shown in Fig. 2. Applying linear Bragg and Vegard's law [20], the x value in the $GaAs_{1-x}N_x$ is determined. The values x= 2.98%, 3.01% and 2.91% are obtained for the samples. The position of the $GaAs_{1-x}N_x$ peak depends on the average nitrogen concentration. As seen in Fig. 2, the peaks for $GaAs_{1-x}N_x$ slightly shift to the right side because of possessing a larger concentration of nitrogen. The diffraction peaks in the XRD pattern can be indexed to the cubic structure of GaAs, which are in good agreement with the standard data for GaAs (JCPDS Card No. 01-088-2489). Accurate results were obtained by simulating the (002) diffraction peaks in Fig. 2.

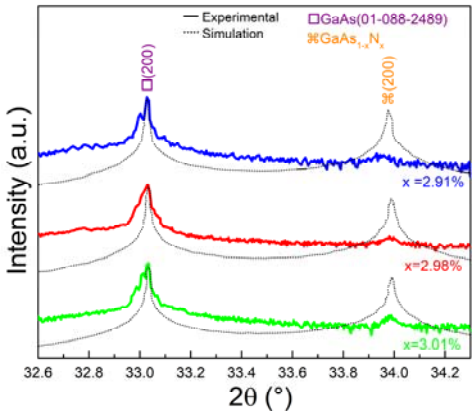

Fig. 2. XRD patterns of the samples

Fig. 3 shows the PL spectra of the samples. As more N is incorporated, the absorption edge slightly shifts to a shorter wavelength, indicating an increase of the band gap energy (E_g). An increase in the peak energy obtained from the PL spectra with increasing nitrogen concentration is negligible due to their similar nitrogen values. By fitting each PL spectrum using a Gaussian distribution function, the peak position of the emission component is obtained. This peak position can be considered to correspond to E_g, the value of which is found to be 1.2701, 1.2703, and 1.2695 eV for the samples with x= 2.98%, 3.01% and 2.91%, respectively. The band gap values obtained from the PL measurements are of the same order of magnitude as found in various systems [20]. No PL in the region of the GaAs band gap may indicate that the higher energy peaks are not from discrete levels in the GaAs.

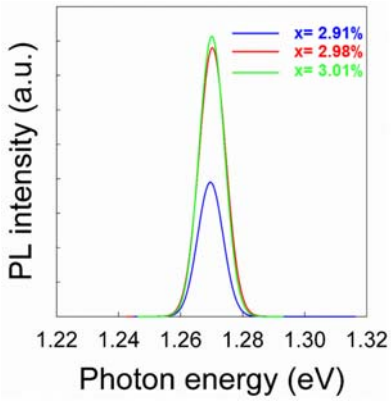

Fig. 3. Room temperature photoluminescence spectra of the samples

To determine the line width of the PL peak, each PL spectrum was fitted by a Gaussian distribution function. The broadening in the PL peak is associated with an inhomogeneous nitrogen concentration in the structure [21]. The value of the line is estimated as 43, 41 and 42 meV for the samples with *x*= 2.98%, 3.01% and 2.91%, respectively. Even though there is almost no difference in the line width of the PL peak, the PL intensity of GaAsN increases significantly for the samples with x=2.98% and x=3.01%. These results demonstrate that the layer structure and the growth conditions of these samples make them suitable candidates for GaAsN (*x*~3%) optical applications.

Fig. 4 depicts a plot of mobility versus temperature. The mobility is thermally activated for the samples with *x*= 2.98% and 3.01% and becomes weakly temperature dependent for the sample with *x*= 2.91%. Hall effect analysis indicates that layer structures and growth conditions significantly affect GaAsN electron mobility. The value of the electron mobility for the sample with *x*= 3.01% grown on SI GaAs substrate was very high in comparison with the other samples, and we should point out that the value of mobility ($3.3x10^4 cm^2/Vs$ at 40 K) for the sample with x= 3.01% is also significantly higher than those of the GaAsN samples reported in the literature [22,23]. On the other hand, the incorporation of Si into GaAsN reduces the mobility of the GaAsN layers grown on SI GaAs (see the sample with *x*= 2.91%). The sample with *x*= 2.98% shows the lowest mobility at room temperature, possibly due to increasing the effective mass for this sample [14]. The scattering mechanisms are shown in the inset of Fig. 4 for the sample with *x*= 2.98%. A similar process was applied to the data of the other two samples (not shown here). Solid curves are drift mobilities for scattering by optical phonons (μ_{po}), dislocations (μ_{dis}), ionized impurities (μ_{ii}), and alloy scattering (μ_{al}). Optical phonon scattering is caused by dipole moments that are due to the interactions between ionic charges and optical lattice vibrations. A lattice mismatch between GaAs and $GaAs_{1-x}N_x$ causes dislocation scattering while the presence of Coulombic forces between mobile carriers and ionized impurity leads to ionized impurity scattering. Finally, alloy scattering and space-charge scattering are due to the presence of an inhomogeneous nitrogen concentration, which was previously confirmed by PL results. The analytical expressions of the scattering mechanisms used in our calculations are given elsewhere [24-30].

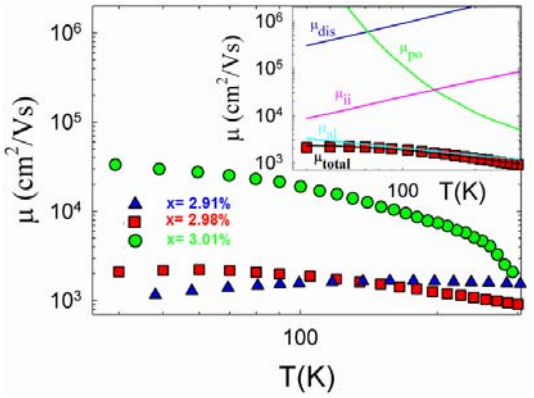

Fig. 4. Hall mobility vs. temperature. Solid curves are drift mobilities for scattering by optical phonons (μ_{po}), dislocations (μ_{dis}), ionized impurities (μ_{ii}), and alloy scattering (μ_{al}). μ_{total} represents the drift mobility in the conduction band calculated using Matthiessen's rule

μ_{total} represents the drift mobility in the conduction band calculated using Matthiessen's rule [30]. The material parameters used in the scattering analyses are given in [29]. Our results suggest that the dominant scattering mechanism is nitrogen-related alloy scattering for the samples with *x*= 2.98% and 2.91% over the whole temperature range. However, its value for the sample with *x*= 2.98% is slightly higher than that of the sample with *x*= 2.91%. For the sample with *x*= 3.01%, we found that space-charge scattering [28] governs mobility at low temperatures, while polar optical phonon scattering is the dominant scattering mechanism at high temperatures (*T* > 200K).

Fig. 5 shows the temperature dependence of the carrier concentration. The carrier concentration data of the samples with x=2.98% and 2.91% are flat over the entire temperature region, denoting a degenerate semiconductor behavior. To further validate that, for the samples with *x*= 2.98% and *x*= 2.91, we consider a critical concentration ($n_c = (0.25/a_B)^3 = 1.8x10^{16}$ cm^{-3} for *x*=3% in $GaAs_{1-x}N_x$, where a_B is Bohr radius) of carrier concentration given for the metal-insulator transition. The carrier concentration values of the samples with *x*= 2.98% and *x*= 2.91% are greater than the n_c, which demonstrates that they exhibit degenerate semiconductor behavior. On the other hand, the sample with *x*= 3.01%, whose carrier concentration thermally increases with $n < n_c$, falls on the insulating side of the metal insulator transition over the whole temperature range. The lower carrier concentration observed for this sample might be due to mobile carrier trapping at N interstitials [21].

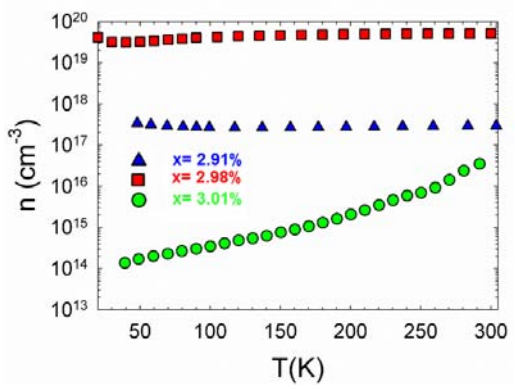

Fig. 5. Temperature dependent Hall carrier density of the samples

We finally investigate the power factor ($PF = S^2ne\mu$). We have already measured n and μ as a function of temperature. However, the Seebeck coefficient (S), which could be used for comparison, was not directly measured. On the other hand, the calculated values of S for both samples are very probable, as we will see. Based on the discussion above, we can see that the Seebeck coefficient of the samples with x= 2.98% and 2.91% can be calculated by a given relationship between carrier concentration and the Seebeck coefficient for degenerate semiconductors [32]:

$$S = \frac{8\pi^2 k_B^2}{3eh^2} m^* T \left(\frac{\pi}{3n}\right)^{\frac{2}{3}} \quad (1)$$

where k_B is Boltzmann's constant, h is Planck's constant, m^* is the effective mass of carriers, and n is the carrier concentration. Note that we are unable to calculate the Seebeck coefficient of the sample with x= 3.01% due to its non-degenerate behavior. It is expected that the sample with x=3.01% has a significantly low *PF* value.

From Eq. (1), it is apparent that the Seebeck coefficient increases according to the reduction in the carrier concentration. Actually, the estimated values of the Seebeck coefficient for the samples with Eq. (1) given in Table 2 are consistent with the experimental findings for GaAsN [33,34].

Table 2. Room temperature values of some parameters

Parameters	**x= 2.98%**	**x= 3.01%**	**x= 2.91%**
x (%)	2.98	3.01	2.91
μ (cm^2/Vs)	909	2090	1538
n (cm^{-3})	5.2x10^{19}	3.5x10^{15}	2.9x10^{17}
σ (Ω cm)$^{-1}$	7519	12	73
S (μV/K)	-9.4	-	-298
PF (μW/mK^2)	66	-	648

Combining these results with the Hall effect results allows us to obtain the temperature dependence of the *PF*s of *sample A* and *sample C*, as shown in Fig. 6. The *PF* increases as the temperature increases for both samples. Compared with the sample with x= 2.98%, the sample with x= 2.91% shows a larger *PF* value both at room and low temperature, owing to its relatively lower carrier concentration and sufficiently high conductivity. As seen from Table II, the room-temperature *PF* value of the sample with x= 2.91% is almost 10 times higher than that calculated for the sample with x= 2.98%. Since the nitrogen content is very similar for the samples, we can consider the layer structure and growth conditions of the samples for comparison. We find it noteworthy that the thermoelectric properties for the GaAsN films with a SI GaAs substrate and Si dopant are excellent. Finally, this conclusion indicates that layer structure and growth conditions are very important for both the material structure quality and possible device performance of GaAsN as a thermoelectric material. Therefore, the layer structure and growth conditions of the sample with x=2.91% might be considered ideal for further investigation of the thermoelectric properties of GaAsN.

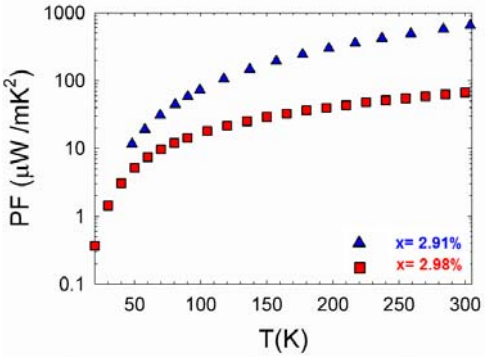

Fig. 6. Temperature dependent power factor (PF) of the samples

4. Conclusions

GaAsN samples were fabricated by MOVPE on semi-insulating (SI) and *n*-type GaAs substrates. The nitrogen content of the samples was approximately 3%. We performed a systematic investigation of the dependence of optical, electrical and thermoelectric properties on the layer structure and growth condition of the samples. The sample with x= 3.01% exhibited the largest PL intensity and had the highest mobility, making it eligible for GaAsN optoelectronic applications. The samples with x= 2.98% and x=2.91% showed a degenerate semiconductor behavior, which is desired for thermoelectric applications. Compared to other materials [8-10], the *PF* of GaAsN was remarkably improved with Si doping (the sample with x= 3.01%). Therefore, with its relatively higher *PF* value, it is a promising candidate for thermoelectric energy harvesters.

Acknowledgements

M. B. would like to acknowledge the help of Dr. Giovanni Attolini and Dr. Nahida Musayeva for the growth of the GaAsN samples. The work is based on Y.Y.'s Ms. thesis.

References

[1] C. Duran, A. Yildiz, S. Dursun, J. Mackey, A. Sehirlioglu, Scripta Materialia **112**, 114 (2016).
[2] G. C. Catlin, R. Tripathi, G. Nunes Jr., P. B. Lynch, H. D. Jones, D. C. Schmit, J. Power Sources **343**, 316 (2017).
[3] A. Yildiz, S. B. Lisesivdin, M. Kasap, D. Mardare, Optoelectron. Adv. Mat. **1**(10), 531 (2007).
[4] A. A. Alsaç, A. Yildiz, T. Serin, N. Serin, Journal of Applied Physics **113**, 063701 (2013).
[5] T. Serin, A. Yildiz, Ş. H. Şahin, N. Serin, Physica B **406**, 575 (2011).
[6] A. M. Dehkordi, M. Zebarjadi, J. He, T. M. Tritt, Materials Science and Engineering R **1**, 97 (2015).
[7] A. Shakouri, S. Li, Thermoelectric Power Factor for Electrically Conductive Polymers, 18th International Conference on Thermoelectrics 402 (1999).
[8] G. Han et al., Angew. Chem. Int. Ed. **55**, 6433 (2016).
[9] L.Wang, Q. Yao, Hui Bi, F. Huang, Q. Wanga, L. Chen, J. Mater. Chem. A, **2**, 11107 (2014).
[10] C. Wan et al, Nature Materials **14**, 622 (2015).
[11] S. B. Lisesivdin, A. Yildiz, M. Kasap, Optoelectron. Adv. Mat. **1**(9), 467 (2007).
[12] S. B. Lisesivdin et al., Journal of Applied Physics **105**, 093701 (2009).
[13] U. Tisch, E. Finkman, J. Salzman, Appl. Phys. Lett. **81**, 463 (2002).
[14] F. Eßer, O. Drachenko, A. Patanè, M. Ozerov, S. Winnerl, H. Schneider, M. Helm, Appl. Phys. Lett. **107**, 062103 (2015).
[15] C. Pelosi, G. Attolini, M. M. Bosi, Avella, C. Calicchio, M.Avella, M. Calicchio, N. Musayeva, J. Jimenez, J. Crystal Growth **287**, 625 (2006).
[16] A. H. Reshak, RSC Adv. **6**, 72286 (2016).
[17] C. Ulyanenkov, International Society for Optics and Photonics **5536,** 1 (2004).
[18] M. Tamer et al., J. Materials Science: Materials in Electronics **27**, 2852 (2016).
[19] D. Zhou, B. F. Usher, J. Phys. D Appl. Phys. **34**, 1461 (2001).
[20] T. S. Kim, T. V. Cuong, C. S. Park, J. Y. Park, H. J. Lee, E.-K. Suh, C.-H. Hong, J. Korean Physical Society **43**, 273 (2003).
[21] K. Uesugi, I. Suemune, T. Hasegawa, T. Akutagawa, T. Nakamura, Appl. Phys. Lett. **76**, 1285 (2000).
[22] A. Moto, S. Tanaka, N. Ikoma, T. Tanabe, S. Takagishi, M. Takagishi, T. Katsuyama, Jpn. J. Appl. Phys. **38**, 1015 (1999).
[23] D. L. Young, J. F. Geisz, T. J. Coutts, Appl. Phys. Lett. **82**, 1236 (2003).
[24] F. Ishikawa, G. Mussler, K.-J. Friedland, H. Kostial, K. Hagenstein, L. Däweritz, K. H. Ploog, Appl. Phys. Lett. **87**, 262112 (2005).
[25] B. K. Ridley, B. E. Foutz, L. F. Eastman, Phys. Rev. B **61**, 16862 (2000).
[26] D. Zanato, S. Gokden, N. Balkan, B. K. Ridley, W. J. Schaff, Semicond. Sci. Technol. **19**, 427 (2004).
[27] D. Zanato, S. Gokden, N. Balkan, B. K. Ridley, W. J. Schaff, Superlattices Microstruct. **34**, 77 (2003).
[28] I. T. Yoon, S. J. Oh, H. L. Park, J. Appl. Phys. **83**, 1527 (1998).
[29] H. Morkoç, Nitride Semiconductors and Devices. Springer-Verlag, Berlin, Heildelberg, New York, 236 (1998).
[30] S. B. Lisesivdin, A. Yildiz, N. Balkan, M. Kasap, S. Ozcelik, E. Ozbay, J. Appl. Phys. **108**, 013712 (2010).
[31] M. Reason, H. A. McKay, W. Ye, S. Hanson, R. S. Goldman, V. Rotberg, Appl. Phys. Lett. **85**, 1692 (2004).
[32] M. Cutler, J. F. Leavy, R. L. Fitzpatrick, Phys. Rev. **133**, A1143 (1964).
[33] P. Pichanusakorn, Y. J. Kuang, C. J. Patel, C. W. Tu, P. R. Bandaru, Appl. Phys. Lett. **99**, 072114 (2011).
[34] T. Dannecker, Y. Jin, H. Cheng, C. F. Gorman, J. Buckeridge, C. Uher, S. Fahy, C. Kurdak, R. S. Goldman, Phys. Rev. B **82**, 125203 (2010).

*Corresponding author: yildizab@gmail.com